Zero-magnetic-field operation of ordinary-Nernst-effect-based transverse thermoelectric module using embedded permanent magnets

Masayuki Murata[1,a)], Takamasa Hirai[2], Takeshi Seki[2,3,4], and Ken-ichi Uchida[2,3,a)]

AFFILIATIONS

[1] National Institute of Advanced Industrial Science and Technology, Tsukuba 305-8568, Japan

[2] National Institute for Materials Science, Tsukuba 305-0047, Japan

[3] Institute for Materials Research, Tohoku University, Sendai 980-8577, Japan

[4] Center for Science and Innovation in Spintronics, Tohoku University, Sendai 980-8577, Japan

[a)] **Authors to whom correspondence should be addressed:** m.murata@aist.go.jp and UCHIDA.Kenichi@nims.go.jp

ABSTRACT

The ordinary Nernst effect enables large transverse thermoelectric conversion in semimetals but its operation requires the application of an external magnetic field. In this study, we propose a transverse thermoelectric conversion module structure with embedded permanent magnets and demonstrate thermoelectric power generation by the ordinary Nernst effect in the absence of an external magnetic field. In our prototype module comprising alternately stacked $Bi_{88}Sb_{12}$ slabs and $Nd_2Fe_{14}B$-type permanent magnets, the stray magnetic field generated by the remanent magnetization of the $Nd_2Fe_{14}B$-type magnets is always applied to the $Bi_{88}Sb_{12}$ slabs, and a power of 13.1 μW is generated due to the ordinary Nernst effect at a temperature difference of 120 K and average temperature of 260 K at zero external field. This thermoelectric module concept will contribute to the further development of transverse thermoelectric conversion technologies utilizing permanent magnets.

The ordinary Nernst effect (ONE) is a transverse thermoelectric conversion phenomenon in a conductor in which an electric field $\mathbf{E}_{ONE}$ is generated in the direction perpendicular to an applied temperature gradient ∇T and magnetic field $\mathbf{H}$, where $\mathbf{E}_{ONE} \propto \mathbf{H} \times \nabla T$. Owing to the orthogonal relation between $\mathbf{E}_{ONE}$ and ∇T, ONE enables thermoelectric generation with a convenient scaling law

and simple junction-less structure, which is different from longitudinal thermoelectric modules based on the Seebeck effect comprising multiple junctions of *p*-type and *n*-type conductors.[1,2] To develop transverse thermoelectric conversion technologies, ONE has been observed in a wide variety of materials and large transverse thermopower has been observed in several Dirac and Weyl semimetals.[3-12] In our previous study, we demonstrated thermoelectric power generation and cooling in an transverse thermoelectric module consisting of semimetallic Bi-Sb alloys, which are known to exhibit large ONE.[13] The ONE-based module was fabricated by four rectangular $Bi_{88}Sb_{12}$ slabs electrically connected through Cu electrodes in series with a zigzag configuration on an AlN substrate. The power generation and cooling characteristics of the ONE-based module were evaluated under external magnetic fields up to 5 T using a superconducting magnet. The maximum output power of the ONE contribution was observed to be 0.319 mW under 5 T with a temperature difference of 149 K. However, applications of ONE are yet to be realized as its operation requires a large external magnetic field. Although this problem can be solved in principle by using the anomalous Nernst effect (ANE) in magnetic materials with finite remanent magnetization, which appears in the absence of a magnetic field,[14-21] the thermopower generated by ANE is much smaller than that by ONE in the Dirac and Weyl semimetals under a magnetic field.

In this study, we propose an ONE-based thermoelectric generation module structure that can operate without the application of an external magnetic field. The module consists of alternately stacked slabs of semimetals exhibiting large ONE and permanent magnets exhibiting large remanent magnetization. The semimetals placed between the permanent magnet slabs are subjected to stray magnetic fields in the direction perpendicular to the stacking plane, which is sustained without the application of an external magnetic field, as shown in Fig. 1(a). Although the magnitude of the stray magnetic fields of the permanent magnets is typically smaller than $\mu_0 H$ = 1 T with μ_0 and H being the vacuum permeability and magnitude of **H**, respectively, large thermoelectric generation can be realized by selecting semimetals that output large transverse thermopower under low magnetic fields. In the previous study, the artificially tilted $Bi_{88}Sb_{12}/Nd_2Fe_{14}B$ multilayer were fabricated to enhance the transverse cooling performance through the magneto-thermoelectric effects in the absence of the external magnetic field.[22] However, this device did not satisfy the symmetry of ONE because of the absence of magnetization component in the direction of the cross product of the heat flow and the electrical current, except near the sample edges with non-uniform stray fields. Thus, in the conventional transverse thermoelectric materials with embedded permanent magnets, the potential of ONE is not fully utilized in the absence of an external magnetic field. Therefore, it would be important to fabricate a device that satisfies the symmetry of ONE by a multilayer with embedded permanent magnets and show that ONE is clearly obtained even in the absence of the external magnetic field.

To demonstrate the concept of the ONE-based transverse thermoelectric module operating at zero external magnetic field, we used semimetallic $Bi_{88}Sb_{12}$ and $Nd_2Fe_{14}B$-type permanent magnet (note that $Bi_{88}Sb_{12}$ can be regarded as a semimetal because all the measurements shown below were performed near room temperature, i.e., > 200 K, while it is a narrow-gap semiconductor at lower temperatures[23-25]). It is known that the transverse thermopower due to ONE in $Bi_{88}Sb_{12}$ near room temperature rises sharply at low magnetic fields below $\mu_0 H$ = 0.5 T. [6,7] This property is useful for demonstrating the usability of the proposed module since the stray fields of permanent magnets is smaller than 1 T. We select the $Nd_2Fe_{14}B$-type magnet because it exhibits the largest remanent magnetization among mass-produced permanent magnet materials. Homogenous $Bi_{88}Sb_{12}$ alloy slabs were prepared with the following processes. First, 99.99% purity $Bi_{88}Sb_{12}$ alloy powder, available from Kojundo Chemical Laboratory Co., Ltd., was crushed using a planetary ball mill (PL-7, Fritsch Japan Co., Ltd) at 350 rpm for 30 minutes. The crushed powder was then sieved through a 63 μm mesh. Next, a cylindrical $Bi_{88}Sb_{12}$ ingot of the 20 mm diameter and ~15 mm thickness was prepared by a spark plasma sintering (SPS) method under a pressure of 50 MPa at 245℃ for 5 minutes in vacuum. The composition difference between the ingot and raw powder was confirmed to be negligibly small by an inductively coupled plasma optical emission spectrometer. As reported in Ref. 25, the Bi-Sb alloy prepared by the SPS method showed no significant difference in XRD patters in the pressurized and its orthogonal directions, and the measured property was explained by assuming random grain crystal orientation.[25] Since our $Bi_{88}Sb_{12}$ alloy was prepared in a similar manner to that used in Ref. 25, we can assume its random grain crystal orientations and isotropic transport properties. The ingot was cut into many rectangular-shaped slabs with a size of 17×6×1 mm^3. To construct the module, we used magnetized $Nd_2Fe_{14}B$-type magnet slabs with a size of 15×5×1 mm^3 with an insulating resin coating on their surface, which are available from Magfine Corporation [note that the black colored slabs in Fig. 1(b) is due to the resin coating]. The 7 $Bi_{88}Sb_{12}$ slabs and 8 $Nd_2Fe_{14}B$-type magnet slabs were alternately stacked so that the magnetization direction of the magnets was aligned in the same direction. Here, the slabs were spontaneously attached to each other due to the magnetic force of the $Nd_2Fe_{14}B$-type magnets. The $Bi_{88}Sb_{12}$ and $Nd_2Fe_{14}B$-type magnet layers were electrically insulated due to the resin coating layers, preventing the reduction of the ONE thermopower by the shunting effect. To increase mechanical strength, the stacked $Bi_{88}Sb_{12}$/$Nd_2Fe_{14}B$-type magnet block was embedded in epoxy resin (EP-3000/EH-3000, PACE Technologies) and degassed in a vacuum, followed by the curing process for 24 hours at room temperature and atmospheric pressure. By using a resin that cures at room temperature, the reduction of the remanent magnetization of the magnet layers can be avoided. Finally, excess resin was removed with a diamond wire saw, and the exposed $Bi_{88}Sb_{12}$ layers were connected in parallel by indium crimping. The size of the constructed module is 16.5×16.8×6.0 mm^3.

To estimate the stray magnetic field applied to the $Bi_{88}Sb_{12}$ layers in the module under zero external field, a dummy sample with holes where a Hall sensor could be inserted at the positions of $Bi_{88}Sb_{12}$ was also prepared and the magnetic field distribution was measured. As shown in Fig. 1(c), a stray magnetic field of $\mu_0 H_s \sim 0.43$ T was applied around the center of the module at room temperature. Although $\mu_0 H_s$ decreases to ~ 0.36 T near the ends of the module, it is large enough to drive ONE of $Bi_{88}Sb_{12}$. Furthermore, H_s in the module at the temperatures ranging from 200 K to 360 K was estimated by correcting the magnetic field distribution under room temperature based on the temperature dependence of the remanent magnetization M_r of the $Nd_2Fe_{14}B$-type magnet, measured with a superconducting quantum interference device magnetometer (MPMS3-SQUID, Quantum Design Inc.). Figure 1(d) displays the magnetization M as a function of H for the $Nd_2Fe_{14}B$-type magnet with a size of $2.1 \times 2.1 \times 1.0$ mm^3, in which **H** was applied along the short axis of the magnet. From these magnetization curves measured at different temperatures, the temperature dependences of the M_r and saturation magnetization M_s were obtained as shown in Fig. 1(e) as well as the coercivity H_c in Fig. 1(f), indicating that high M_r/M_s and sufficiently large H_c are maintained even at 360 K.

Figure 2 represents the external magnetic field H dependence of the thermo- and galvano-magnetic properties of a single $Bi_{88}Sb_{12}$ slab prepared by the same procedure as that for the elements used in the module, at magnetic fields from 0 to 5 T and temperatures ranging from 200 K to 360 K. The measurement of the transport properties was performed in the same manner as the previous report.[6,7,27] The ONE thermopower S_{ONE} at all temperatures decreased once by increasing the magnetic field from 0 T, exhibiting the minimum values from −18.3 μV K^{-1} (around 0.4 T at 200 K) to −13.2 μV K^{-1} (around 1.3 T at 360 K). Importantly, the S_{ONE} value of $Bi_{88}Sb_{12}$ changes sharply at low magnetic fields, and a large magnitude of the thermopower is achieved around 0.4 T which can be generated by the stray magnetic field of the $Nd_2Fe_{14}B$-type magnets. The value of S_{ONE} of the prepared $Bi_{88}Sb_{12}$ alloy is comparable to that of single crystalline Bi or Bi-Sb alloys at low magnetic fields of <0.4 T around room temperature.[28,29] On the other hand, the magnitude of the Seebeck coefficient S shown in Fig. 2(b) increased monotonically with H at all temperatures due to the ordinary magneto-Seebeck effect. The diagonal resistivity ρ shown in Fig. 2(c) increased monotonically with the magnetic field due to the ordinary magnetoresistance effect. These results were consistent with those reported on $Bi_{88}Sb_{12}$ alloys prepared by a similar procedure using the SPS method.[6,7]

We next investigated the thermoelectric power generation characteristics of the constructed module. As heat baths, two AlN substrates with dimensions of $21 \times 23 \times 0.5$ mm^3 were fixed on the hot- and cold- side surfaces of the module using silicone adhesive (1225B, ThreeBond Co., Ltd.). The temperature difference between the hot- and cold-side heat baths was measured with a 25-μm diameter T-type differential thermocouple (Omega Engineering, Inc.) attached to the two AlN

substrates. In order to apply a temperature difference to the module, the cold-side heat bath was secured to a sample stage of a Gifford-McMahon cryocooler with silicone grease (MOLYKOTE High Vacuum Grease, DuPont Toray Specialty Materials K.K.), and a 25-mm-square and 1.8-mm-thick ceramic heater (MC2525, Sakaguchi Electric Heaters Co., Ltd.) was fixed to the hot-side heat bath with the same silicone grease. The module and heater were secured to the sample stage with fluorinated ethylene propylene heat-shrinkable tubing (NF300, Junkosha Inc.) to prevent the module from moving in external magnetic fields. The temperature of the sample stage was measured with a platinum resistance thermometer (PT-100) and controlled with a heater embedded in the sample stage, using a temperature controller (336, Lake Shore Cryotronics Inc.). The temperature difference within the module was determined from the voltage of the differential thermocouple measured with a nanovoltmeter (2182, Keithley) and the sample stage temperature. The desired temperature difference was obtained by applying the appropriate current to the hot-side heater using a current source (PSW-1080L80, TEXIO TECHNOLOGY Corp.). The power generation characteristics of the module were evaluated under three conditions at the hot- and cold-side temperature: i) 275 K and 325 K (ΔT = 50 K, $\overline{T}$ = 300 K), ii) 240 K and 360 K (ΔT = 120 K, $\overline{T}$ = 300 K), and iii) 200 K and 320 K (ΔT = 120 K, $\overline{T}$ = 260 K), where ΔT and $\overline{T}$ are the temperature difference and average temperature in the module, respectively. A magnetic field ranging from –5 to +5 T was applied using a superconducting magnet (Cryogen Free Magnet System, Cryogenic Ltd.). All measurements were conducted in a vacuum of less than 10^{-3} Pa.

The magnetic field dependence of the open-circuit voltage V_{open} measured with a digital multimeter (2002, Keithley) under three temperature conditions is shown by the black lines in Figs. 3(a),(b). The solid and dotted lines represent the magnetic field dependence of V_{open} when the magnetic field is changed from negative to positive ($V_{\mathrm{open,f}}$) and from positive to negative ($V_{\mathrm{open,b}}$), respectively. The measured V_{open} includes not only ONE but also the Seebeck thermopower due to a lateral temperature non-uniformity in the module. These two thermopower contributions can be separated as $V_{\mathrm{open,f,N}}(H) = \{V_{\mathrm{open,f}}(+H)-V_{\mathrm{open,b}}(-H)\}/2$ and $V_{\mathrm{open,b,N}}(H) = \{V_{\mathrm{open,f}}(-H)-V_{\mathrm{open,b}}(+H)\}/2$ for ONE, and $V_{\mathrm{open,f,S}}(H) = \{V_{\mathrm{open,f}}(+H)+V_{\mathrm{open,b}}(-H)\}/2$ and $V_{\mathrm{open,b,S}}(H) = \{V_{\mathrm{open,f}}(-H)+V_{\mathrm{open,b}}(+H)\}/2$ for the Seebeck effect, by considering their symmetry with respect to the magnetic field. The magnetic field dependence of V_{open} for the ONE and Seebeck effect components in the range of $\mu_0|H| \leq 1$ T are shown by the red and blue lines in Fig. 3(a), respectively. These curves exhibit hysteresis, which does not correspond to the ONE or Seebeck effect of the single $Bi_{88}Sb_{12}$ slab. This hysteresis was caused by the large coercivity of the $Nd_2Fe_{14}B$-type magnets which applies the stray magnetic field to the $Bi_{88}Sb_{12}$ elements. The values of $V_{\mathrm{open,f,N}}$ and $V_{\mathrm{open,b,N}}$ at 0 T were the same absolute values with opposite signs: i) ±0.49 mV, ii) ±1.1 mV, and iii) ±0.91 mV, clearly indicating that the output voltage

was successfully obtained by ONE without the external magnetic field. The H dependence of the open circuit voltage and its ONE and Seebeck effect components between –5 T and +5 T, shown in Fig. 3(b), indicate that the ONE contribution increased with increasing $|H|$. The H dependence of the module internal resistance R_{in}, measured using a lock-in amplifier (850, Stanford research systems) with an alternating current of 1 mA and 1.234 Hz applied by a current source (6221, Keithley), is also shown in Fig. 3(b) by the green lines. The H dependence of R_{in} also exhibits hysteresis, with minimum values appearing around ±0.4 T. The additional electrical resistance R_{add} of R_{in} outside of the Bi-Sb elements can be estimated using the measured H dependence of ρ of the single $Bi_{88}Sb_{12}$ slab at the same temperature as the average temperature of the module, considering that the resistance outside of the elements, indium and lead wires, in this temperature range is independent of H:

$$R_{\mathrm{add}} = \frac{b\,R_{\mathrm{in,min}} - R_{\mathrm{in,5T}}}{b-1}$$

where b, $R_{\mathrm{in,min}}$, and $R_{\mathrm{in,5T}}$ represent the ratio of ρ at 5 T to that at the minimum ($\rho_{5\mathrm{T}}/\rho_{\mathrm{min}}$), R_{in} at the minimum, and R_{in} at 5 T, respectively. The values of R_{add} at 260 K and 300 K were estimated to be 16 mΩ and 18 mΩ, respectively.

In Fig. 4, we summarize the measured power generation characteristics at ±0 T (the plus-minus sign means that H was changed from +5 T for "+" or –5 T for "–") and ±5 T for the three temperature conditions. Figure 4(a) represents the dependence of the output voltage V_{out} measured with the digital multimeter (2002, Keithley) on the load current I_{load} controlled by a source measure unit (2450, Keithley) at ±0 T and ±5 T. Because the sign of the output voltage changes depending on the temperature conditions and magnetic field, the quadrants in which power generation was obtained differ in this graph. Figure 4(b) represents the I_{load} dependence of the output power P_{out} (= $I_{\mathrm{load}}\times V_{\mathrm{out}}$) at ±0 T and ±5 T. The asymmetry of P_{out} for positive and negative magnetic fields is attributed to the contribution of the Seebeck effect. The combination of the ONE and Seebeck effects is expected to be achieved by satisfying the symmetry of ONE in artificially tilted semimetal/magnet multilayers similar to the previous work.[22] Figure 4(c),(d) represents the I_{load} dependence of the output voltage and power for only the ONE contribution at 0 T and 5 T, separated considering the symmetry of the ONE and Seebeck effect thermopower as: $V_{\mathrm{out,5T,N}}(I_{\mathrm{load}}) = V_{\mathrm{out,+5T}}(I_{\mathrm{load}}) - \{V_{\mathrm{out,+5T}}(I_{\mathrm{load}} = 0\ \mathrm{A}) + V_{\mathrm{out,-5T}}(I_{\mathrm{load}} = 0\ \mathrm{A})\}/2$, $P_{\mathrm{out,5T,N}}(I_{\mathrm{load}}) = V_{\mathrm{out,5T,N}}(I_{\mathrm{load}})\times I_{\mathrm{load}}$, and $V_{\mathrm{out,0T,N}}(I_{\mathrm{load}}) = V_{\mathrm{out,-0T}}(I_{\mathrm{load}}) - \{V_{\mathrm{out,-0T}}(I_{\mathrm{load}} = 0\ \mathrm{A}) + V_{\mathrm{out,+0T}}(I_{\mathrm{load}} = 0\ \mathrm{A})\}/2$, $P_{\mathrm{out,0T,N}}(I_{\mathrm{load}}) = V_{\mathrm{out,0T,N}}(I_{\mathrm{load}})\times I_{\mathrm{load}}$, respectively. The maximum output power $P_{\mathrm{out,max}}$ derived from ONE at 0 T were i) 2.49 μW, ii) 13.1 μW, and iii) 10.4 μW, while those at 5 T were i) 0.131 mW, ii) 0.568 mW, and iii) 1.08 mW. The values of $P_{\mathrm{out,max}}$ normalized with the device area were i) 8.98×10^{-3} W m^{-2}, ii) 4.73×10^{-2} W m^{-2}, and iii) 3.75×10^{-2} W m^{-2} at 0 T, and i) 4.72×10^{-1} W m^{-2}, ii) 2.05 W m^{-2}, and iii) 3.90

W m^{-2} at 5 T, and the values of $P_{out,max}$ normalized with the applied temperature difference[30] were i) 3.59×10^{-3} W m^{-2} K^{-2}, ii) 3.28×10^{-3} W m^{-2} K^{-2}, and iii) 2.60×10^{-3} W m^{-2} K^{-2} at 0 T, and i) 1.89×10^{-1} W m^{-2} K^{-2}, ii) 1.42×10^{-1} W m^{-2} K^{-2}, and iii) 2.70×10^{-1} W m^{-2} K^{-2} at 5 T. This indicates that we have successfully fabricated and demonstrated the transverse thermoelectric power generation module driven by ONE without the application of an external magnetic field. ANE modules can also operate without an external magnetic field, with the record-high output power of 177 μW when using bulk elements suitable for practical use.[20] Although the present ONE-based module using the $Nd_2Fe_{14}B$-type magnets showed lower output power than the ANE-based module, the performance of the ONE-based module can be improved further by increasing the fill factor of the $Bi_{88}Sb_{12}$ slabs showing the transverse thermopower and reducing the contact electrical resistance. The fill factor of the $Bi_{88}Sb_{12}$ slabs in the present module was ~40%, which was approximately half that of the reported ANE-based module.[20] The internal resistance of the present module was more than 10 times higher than the resistance estimated only from the bulk electrical resistivity of the $Bi_{88}Sb_{12}$ slabs. Therefore, by improving these factors, the maximum output power of the ONE-based module is expected to be > 200 μW at 0 T. In order to obtain higher output power from thermoelectric modules, it is desirable to suppress heat flow through areas other than the power generating elements. The heat flow in the fabricated module was simulated using the finite element method with COMSOL Multiphysics 4.4 (see details in the supplementary material). The simulated total thermal conductivity of the module is 3.5 W m^{-1} K^{-1} which is smaller than that of the $Bi_{88}Sb_{12}$ alloy. Even though the thermal conductivity of $Nd_2Fe_{14}B$-type magnets is higher than that of Bi-Sb alloys, the heat through the magnets is not dominant because the magnets are covered with epoxy resin which has the low thermal conductivity.

In conclusion, a transverse thermoelectric conversion module structure with embedded permanent magnets has been proposed and thermoelectric power generation by ONE has been demonstrated in the absence of an external magnetic field. In the prototype module consisting of many alternately stacked $Bi_{88}Sb_{12}$ slabs and $Nd_2Fe_{14}B$-type permanent magnet slabs, the stray magnetic field generated by the remanent magnetization of the magnets is applied to the $Bi_{88}Sb_{12}$ slabs, enabling the emergence of ONE without an external field. In this prototype module, we observed a ONE-driven thermoelectric power of 13.1 μW at a temperature difference of 120 K and average temperature of 260 K at zero external field. This thermoelectric module structure is very robust and can be used for any combinations of semimetals and permanent magnets. If permanent magnet layers exhibit large ANE, hybrid thermoelectric conversion based on ONE and ANE would also be possible. Although we have focused on the thermoelectric generation based on ONE in this study, the same module concept is applicable to thermal management devices based on the ordinary Ettingshausen effect, which is the Onsager reciprocal of ONE. Thus, developing materials with large

transverse thermopower operating at low magnetic fields is important for realizing not only thermal energy harvesting but also electronic cooling applications based on the transverse thermoelectrics.

The authors thank Y. Sakuraba, H. Sepehri-Amin, and Y. Oikawa for valuable discussions and K. Suzuki, M. Isomura, and K. Aoyama for technical supports. This work was supported by CREST "Creation of Innovative Core Technologies for Nano-enabled Thermal Management" (JPMJCR17I1) and ERATO "Magnetic Thermal Management Materials" (JPMJER2201) from JST, Japan, "Mitou challenge 2050" (P14004) from NEDO, KAKENHI Grant-in-Aid for Scientific Research(C) (22K04232) from JSPS, and ACT-X (JPMJAX21KI) from JST, Japan.

DATA AVAILABILITY

The data that support the findings of this study are available from the corresponding author upon reasonable request.

REFERENCES

[1] K. Uchida and J. P. Heremans, Joule **6**, 2240-2245 (2022).

[2] M. Chen, J. Wang, K. Liu, W. Fan, Y. Sun, C. Felser, T. Zhu, C. Fu, Adv. Ener. Mater., 2400411 (2024).

[3] T. C. Harman, J. M. Honig, S. Fischler, and A. E. Paladino, Solid-State Electron. **7**, 505-508 (1964).

[4] S. N. Shabde: The hall and Nernst effect in Bi and Bi-Sb alloys, Rice University, Ph.D. thesis, (1967).

[5] M. Murata, K. Nagase, K. Aoyama, and A. Yamamoto, Appl. Phys. Lett. **117**, 103903 (2020).

[6] K. Uchida, M. Murata, A. Miura, R. Iguchi, Phys. Rev. Lett. **125**, 106601 (2020).

[7] M. Murata, K. Nagase, K. Aoyama, N. Abe, and A. Yamamoto, J. Appl. Phys. **134**, 215103 (2023).

[8] T. Liang, J. Lin, Q. Gibson, T. Gao, M. Hirschberger, M. Liu, R. J. Cava, and N. P. Ong, Phys. Rev. Lett. **118**, 136601 (2017).

[9] G. Sharma, C. Moore, S. Saha, and S. Tewari, Phys. Rev. B **96**, 195119 (2017).

[10] J. Xiang, S. Hu, M. Lyu, W. Zhu, C. Ma, Z. Chen, F. Steglich, G. Chen, and P. Sun, Sci. China Phys. Mech. Astron. **63**, 237011 (2020).

[11] T. Feng, P. Wang, Z. Han, L. Zhou, Z. Wang, W. Zhang, Q. Liu, and W. Liu, Energy Environ. Sci. **16**, 1560-1568 (2023).

[12] Y. Goto, H. Usui, M. Murata, J. E. Goldberger, J. P. Heremans, C.-H. Lee, Chem. Mater. **36**, 2018-2026 (2024).

[13] M. Murata, K. Nagase, K. Aoyama, A. Yamamoto, and Y. Sakuraba, iScience 24, 101967 (2021).

[14] Y. Sakuraba, Scr. Mater. **111**, 29-32 (2016).

[15] M. Ikhlas, T. Tomita, T. Koretsune, M. T. Suzuki, D. Nishio-Hamane, R. Arita, Y. Otani, and S. Nakatsuji, Nat. Phys. **13**, 1085-1090 (2017).

[16] A. Miura, H. Sepehri-Amin, K. Masuda, H. Tsuchiura, Y. Miura, R. Iguchi, Y. Sakuraba, J. Shiomi, K. Hono, K. Uchida, Appl. Phys. Lett. **115**, 222403 (2019).

[17] A. Miura, K. Masuda, T. Hirai, R. Iguchi, T. Seki, Y. Miura, H. Tsuchiura, K. Takanashi, and K. Uchida, Appl. Phys. Lett. **117**, 082408 (2020).

[18] W. Zhou and Y. Sakuraba, Appl. Phys. Exp. **13**, 043001 (2020).

[19] R. Modak, Y. Sakuraba, T. Hirai, T. Yagi, H. Sepehri-Amin, W. Zhou, H. Masuda, T. Seki, K. Takanashi, T. Ohkubo, and K. Uchida, Sci. Technol. Adv. Mater. **23**, 767-782 (2022).

[20] F. Ando, T. Hirai, and K. Uchida, APL Energy **2**, 016103 (2024).

[21] K. Uchida, W. Zhou, and Y. Sakuraba, Appl. Phys. Lett. **118**, 140504 (2021).

[22] K. Uchida, T. Hirai, F. Ando, and H. Sepehri-Amin, Adv. Ener. Mater. **14**, 2302375 (2024).

[23] B. Lenoir, H. Scherrer, and T. Caillat, Semicond. Semimet. **69**, 101-137 (2001).

[24] K. Vandaele, M. Otsuka, Y. Hasegawa, and J. P. Heremans, J. Phys.: Condens. Mater. **30**, 403001 (2018).

[25] S. Gao, J. Gaskins, X. Hu, K. Tomko, P. Hopkins, and S. J. Poon, Sci. Rep. **9**, 14892 (2019).

[26] M. Murata, A. Yamamoto, Y. Hasegawa, and T. Komine, J. Electron. Mater. **45**, 1875-1885 (2016).

[27] M. Murata, M. Suzuki, K. Aoyama, K. Nagase, H. Ohshima, A. Yamamoto, Y. Hasegawa, T. Komine, J. Thermoelectrics Soc. Jpn. **20**, 67-74 (2023). (in Japanese)

[28] S.N. Shabde, The hall and Nernst effect in Bi and Bi-Sb alloys, Rice University Ph.D. thesis, 1967.

[29] B. S. Farag and S. Tanuma, ISSP Technical Report, Ser. B No. 18, 1976.

[30] F. Zhang, Y. Zang, D. Huang, C. Di, D. Zhu, Nat. Commun. **6**, 8356 (2015).

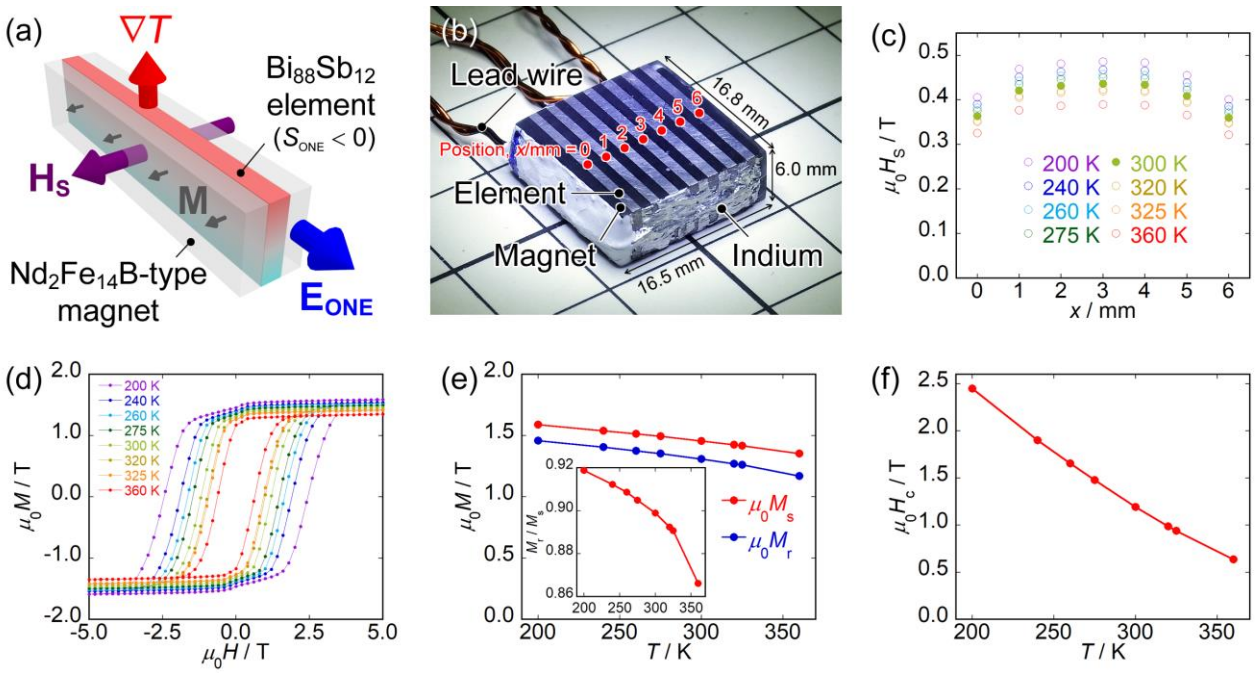

FIG. 1. (a) Schematic of ONE-based transverse thermoelectric conversion operating without the application of an external magnetic field. (b) Photograph of the constructed ONE-based module. (c) Position x dependence of H_s measured in holes of the dummy sample at 300 K (closed circles) and estimated at the other temperatures from the T dependence of M_r (open circles). (d) H dependences of M, (e) T dependence of M_r, M_s, and M_r/M_s (inset), and (f) T dependence of H_c, for the $Nd_2Fe_{14}B$-type magnet.

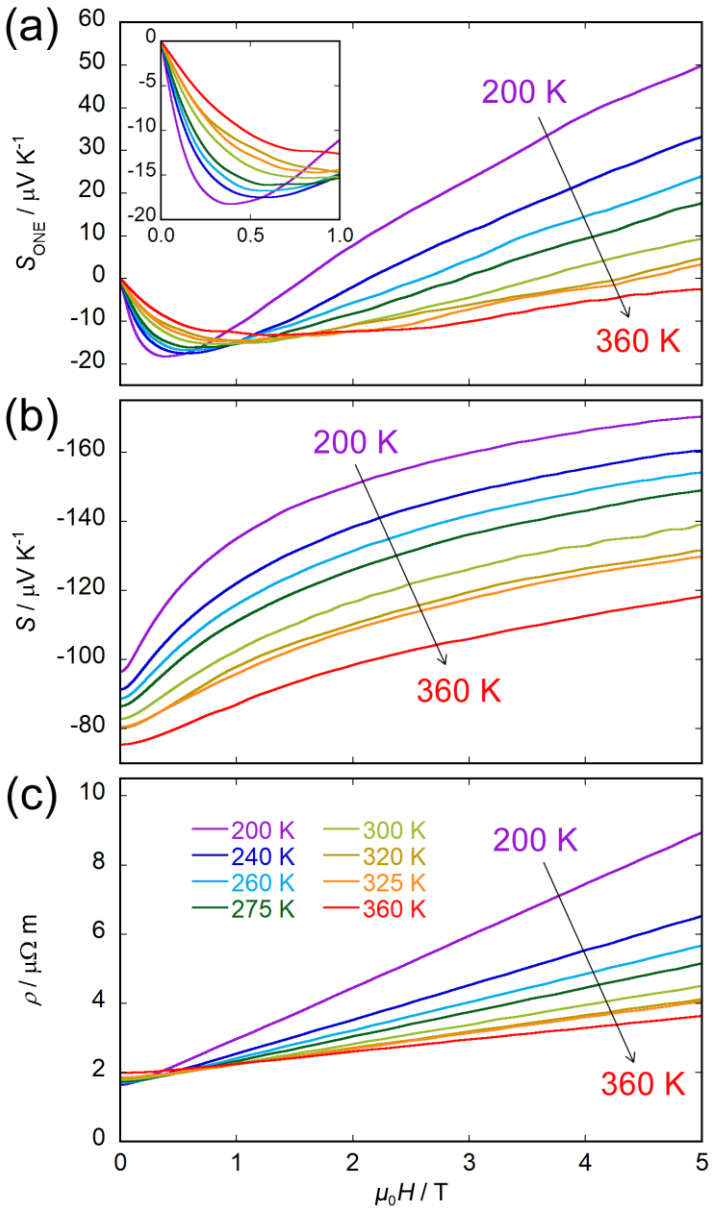

FIG. 2. *H* dependence of (a) S_{ONE}, (b) *S*, and (c) ρ of the single $Bi_{88}Sb_{12}$ slab up to 5 T for various values of *T*.

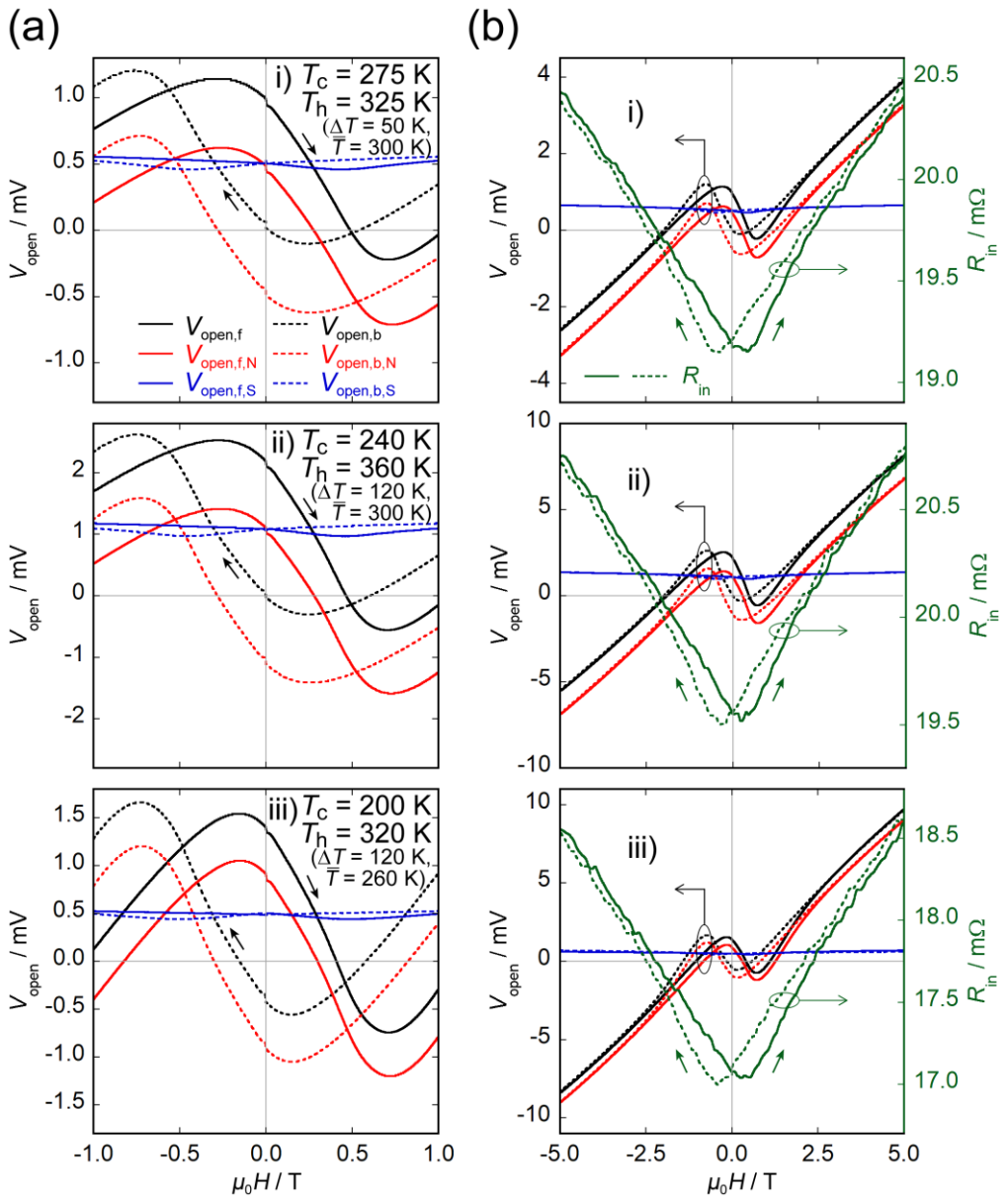

FIG. 3. *H* dependence of $V_{open,f}$ and $V_{open,b}$ (black lines), $V_{open,f,N}$ and $V_{open,b,N}$ (red lines), and $V_{open,f,S}$ and $V_{open,b,S}$ (blue lines) at (a) $-1 \leq \mu_0 H \leq 1$ T and (b) $-5 \leq \mu_0 H \leq 5$ T for the three temperature conditions. In (b), *H* dependence of R_{in} is shown by the green lines.

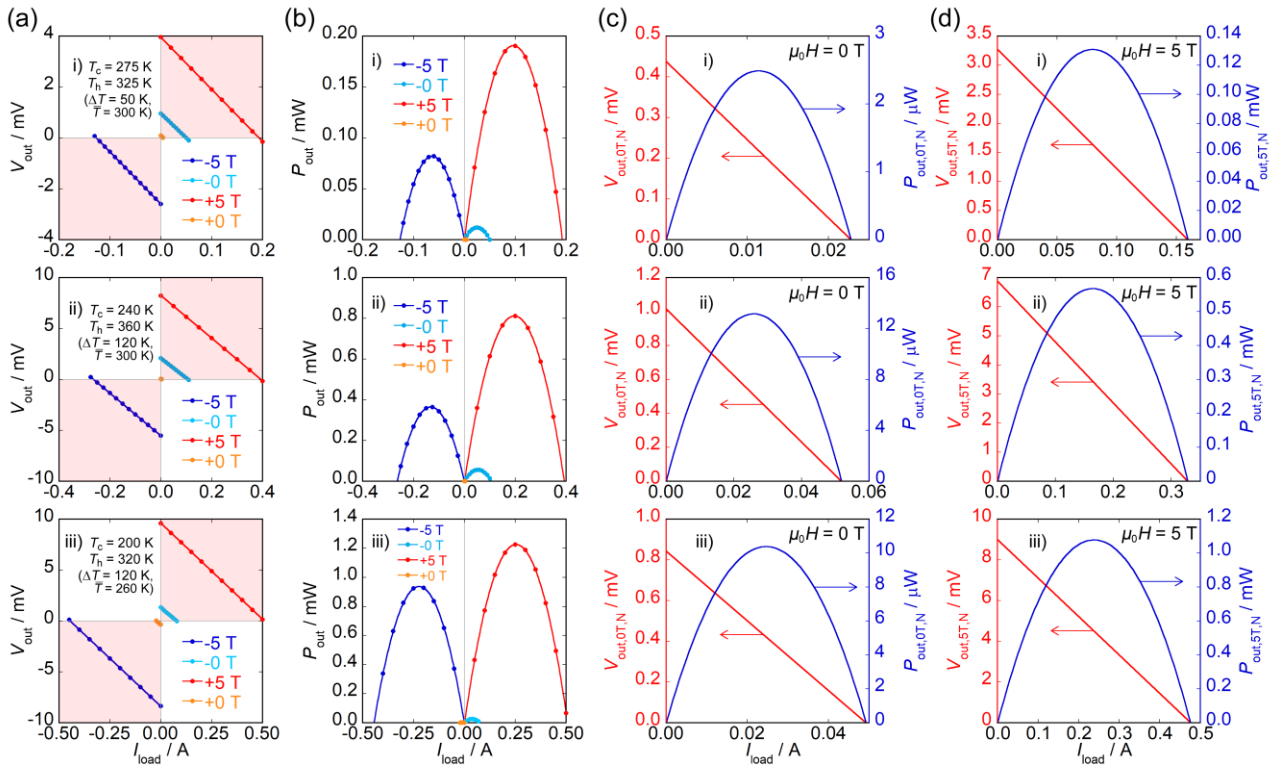

FIG. 4. Measured I_{Load} dependence of (a) V_{out} and (b) P_{out} at ±0 T and ±5 T and evaluated I_{Load} dependence of V_{out} and P_{out} for only the ONE contribution at (c) 0 T and (d) 5 T for the three temperature conditions.